Advances in Concrete Construction, *Vol. 5, No. 2 (2017) 117-143*
DOI: https://doi.org/10.12989/acc.2017.5.2.117

Influence of corrosive phenomena on bearing capacity of RC and PC beams

Pier Giorgio Malerba[1a], Luca Sgambi[*2], Diego Ielmini[1b] and Giordano Gotti[1c]

[1]*Department of Civil and Environmental Engineering, Politecnico di Milano, Milano, Italy*
[2]*Faculty of Architecture, Architectural Engineering and Urbanism (LOCI), Université catholique de Louvain, Louvain-la-Neuve, Belgium*

(Received February 25, 2017, Revised March 3, 2017, Accepted April 13, 2017)

Abstract. The attack of environmental aggressive agents progressively reduces the structural reliability of buildings and infrastructures and, in the worst exposition conditions, may even lead to their collapse in the long period. A change in the material and sectional characteristics of a structural element, due to the environmental damaging effects, changes its mechanical behaviour and varies both the internal stress redistribution and the kinematics through which it reaches its ultimate state. To identify such a behaviour, the evolution of both the damaging process and its mechanical consequences have to be taken into account. This paper presents a computational approach for the analysis of reinforced and prestressed concrete elements under sustained loading conditions and subjected to given damaging scenarios. The effects of the diffusion of aggressive agents, of the onset and development of the corrosion state in the reinforcement and the corresponding mechanical response are studied. As known, the corrosion on the reinforcing bars influences the damaging rate in the cracking pattern evolution; hence, the damage development and the mechanical behaviours are considered as coupled phenomena.

The reliability of such an approach is validated in modelling the diffusion of the aggressive agents and the changes in the mechanical response of simple structural elements whose experimental behaviour is reported in Literature.

A second set of analyses studies the effects of the corrosion of the tendons of a P.C. beam and explores potentially unexpected structural responses caused by corrosion under different aggressive exposition. The role of the different types and of the different positions of the damaging agents is discussed. In particular, it is shown how the collapse mode of the beam may switch from flexural to shear type, in case corrosion is caused by a localized chloride attack in the shear span.

Keywords: corroded R.C. and P.C. beams; time-variant bending and shear capacity; carbonation; chloride attack; corrosion

1. Introduction

*Corresponding author, Assistant Professor, E-mail: luca.sgambi@uclouvain.be
[a]Full Professor, E-mail: piergiorgio.malerba@polimi.it
[b]Structural Engineer, E-mail: diego.ielmini@virgilio.it
[c]Structural Engineer, E-mail: giordano.gotti@hotmail.com

http://www.techno-press.org/?journal=acc&subpage=7 ISSN: 2287-5301 (Print), 2287-531X (Online)

in modelling the load path for P.C. beams under a different aggressive exposition. The role of the different types and of the different positions of the damaging causes is discussed. A result, which is worth outlining, concerns the case of a localised chloride attack in the shear span of P.C. beams. For such a case, it is shown how the corrosion could switch the collapse mode from a flexural collapse to a shear one.

The paper concludes in outlining the modelling capabilities of the proposed approach and in presenting its wide range of application.

2. Characterisation of the damaging environment

2.1 General aspects

Degradation affects both concrete and steel and it is highly dependent on the processes by which the water and the potential aggressive agents (carbon dioxide, chlorides, sulphates, etc.) migrate from the external environment into the concrete mass (Coronelli *et al.* 2009, Lu *et al.* 2016, Michel *et al.* 2016).

These processes are not instantaneous; they occur gradually over a period of time and are influenced by the characteristics of the ambience and of the materials.

With respect to the ambience, we can distinguish between physical factors (the seasonal ranges of temperature and of humidity conditions), and the chemical ones (Ekolu 2016). Among these, in particular, the CO_2 percentage present in the air and the chloride and sulphates concentration in exposed surfaces are considered.

As regards to the materials, the durability of the concrete is strongly influenced by the water-cement ratio and by the cement content. The steels durability depends on their type and grade, being known that the stress corrosion phenomenon makes the prestressing steels more vulnerable to corrosion with respect to the ordinary ones (Tuutti 1982, Nürnberger 2002, Bertolini *et al.* 2004). Special additives may improve the basic characteristics of the concrete. In some applications, special surface protections, like resins and zinc coatings, may improve the steels performance over time.

Other damaging phenomena are of mixed type (physical/chemical/mechanical), as in the case of the relative influence among alkali-silica reactions, freezing and thawing cycles, repeated loading effects and crack propagation. Such kind of processes widens the preferential paths through which the aggressive agents diffuse in the concrete mass and accelerates corrosion and damage of the structural element (Vesikari 1988, Breysse 1997, Vořechovská 2009).

In the development of these damaging processes, two different phases must be identified and clearly distinguished: the incubation time, during which the external aggressive agents penetrate into the concrete cover and cause a progressive destruction of the protective film formed around the bars in an alkaline environment, and the onset and the propagation of corrosion (Tuutti 1982).

2.2 Definition of damaging environment

In the following, the typical microclimate conditions, which surround the bridges girders, will be considered. The external surfaces of the structural elements of a girder are exposed to the carbon dioxide present in the atmosphere, which, interacting with the calcium hydroxide of the concrete, triggers the carbonation. The exposure conditions may be different, but the carbonation

for compact concretes, with a cement contents greater than 3.50 kN/m^3; 5<*K*<8 for medium compactness concretes; *K*>8 for poor concretes, with cement contents below 2.50 kN/m^3.

Cracked concrete. When the tensile stress exceeds the corresponding strength, concrete cracks. The total tensile stress may be the result of different contributions: mechanical, due to the acting loads; distortional, due to creep and shrinkage; environmental, due to temperature exposition or to freezing-thawing cycles.

Carbonation penetration is higher through cracks. According to Vesikari (1988), the carbonation depth is computed through the following equation, which also takes into account the crack width

$$x(t) = 50 \cdot \sqrt{w} \cdot \sqrt[4]{t} \tag{3}$$

In this relationship $x(t)$ is the thickness of the carbonised layer (mm), w is the width of the crack (mm) and t is the time (years). If no aggressive agents are present, the cracking reduces the stiffness of a structural element, but it does not influence its ultimate bearing capacity. In the service ambience, cracks foster the penetration of carbon dioxide and reduce the corrosion initiation time of steel. Hence, a sound evaluation of carbonation depth and carbonation velocity has to take into account the mechanical response of the structure.

2.3.2 Chloride diffusion model

The time required to reach a critical chloride concentration C_{cr} on the reinforcement surface depends on the chloride concentration on the concrete external surfaces, on the cement matrix characteristics, on the thickness of the concrete cover, and on the cracking state. The critical value C_{cr} ranges from 0.4% to 1% in mass with respect to the cement contents. An average value for well compacted concretes is 0.6%.

Uncracked concrete. Considering uncracked concrete as a porous material and chloride propagation as a diffusion process, a close approximation of chloride concentration profiles over time is predicted by Fick's second law, according to the differential equation that follows

$$\frac{\partial C(x,t)}{\partial t} = \frac{\partial}{\partial x}\left[D(x,t) \cdot \frac{\partial C(x,t)}{\partial x} \right] \tag{4}$$

where x is the penetration depth, measured from the reference external surface (mm), t is the time (years), $C(x,t)$ is the chloride concentration (mass % with respect to the cement contents) and $D(x,t)$ is the diffusion coefficient (mm^2/sec).

An analytical solution of Eq. (4), can be obtained if we assume that the chloride content on the external surface C_s remains constant over time and that the diffusion coefficient $D(x,t)=D_{app}$ remains constant over time and in the space. Under these hypotheses, the concentration of chlorides at the depth x and at the time t is given by following equation

$$C(x,t) = C_s \left[1 - erf\left(\frac{x}{2 \cdot \sqrt{D_{app} \cdot t}} \right) \right] \tag{5}$$

where *erf* is the Gauss error function and $D_{app}=10^{-7} \div 10^{-5}$ (mm^2/s) is the so called apparent (effective) diffusion coefficient. This equation can be used to determine when the critical chloride concentration is reached and steel corrosion starts.

Cracked concrete. In the design practice, the diffusion coefficient may be assumed as constant, even if it actually depends on many chemical, physical and mechanical phenomena, which vary

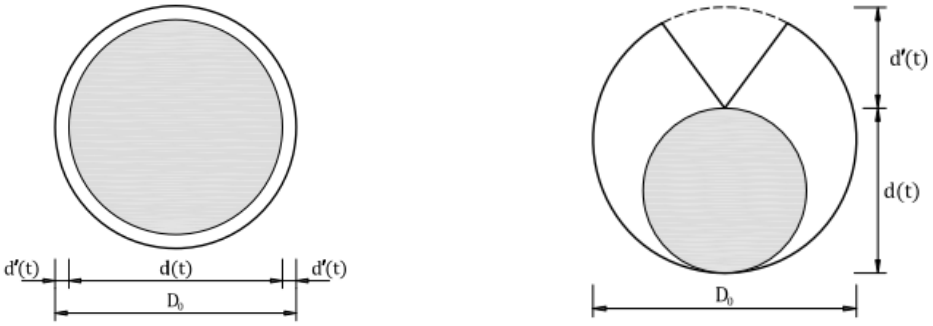

(a) (b)

Fig. 1 Geometry of the corroded reinforcing bar, (a) uniform corrosive attack and (b) corrosive attack on one side only

By reinforcement degradation we mean a reduction of the cross-sectional area of the bars without changes of their Young's modulus. Moreover, the corrosion phenomenon depends on the aforementioned environmental conditions, on the material characteristics and on the integrity of the concrete volume.

Several models are presented in the RILEM Report 14 (Sarja and Vesikari 1996). The most widely used gives the effective area of reinforcement $A_s(t)$ (mm^2), reduced by corrosion, as follows

$$A_s = \begin{cases} \dfrac{N_s \cdot \pi \cdot D_0^2}{4} & if \quad t \le t_0 \\ \dfrac{N_s \cdot \pi \cdot \left[D_0 - n \cdot d'(t) \right]^2}{4} & if \quad t > t_0 \end{cases} \tag{8}$$

where N_s is the number of reinforcing bars, D_0 is their initial diameter (mm), $d'(t)$ is the depth of corrosion (Fig. 1) (mm), t_0 is the time of corrosion initiation (years), n=(1, 2) is a coefficient that takes into accounts the possibility of the attack coming from one or two sides of the reinforcing bar.

At the time t, the depth of the corrosion of the corroded reinforcing bar $d'(t)$, which appears in Eq. (8), is estimated through Faraday's law

$$d'(t) = 0.0116 \cdot i_{corr} \cdot (t - t_0) \tag{9}$$

where i_{corr} is the corrosion current per unit area (μA/cm^2), t is the total time (years) since the completion of the building and 0.0116 is a conversion factor from μA/cm^2 to μm/year. According to this formulation of Faraday's law and in the case of steel, a corrosion current of 1 μA/cm^2 corresponds to a diameter decrease of 11.60 μm/year.

Then, reinforcing bar diameter $d(t)$, as function of time, can be estimated as

$$d(t) = D_0 - n \cdot d'(t) \tag{10}$$

and results linear over time.

2.4.2 Corrosion model for prestressing reinforcement

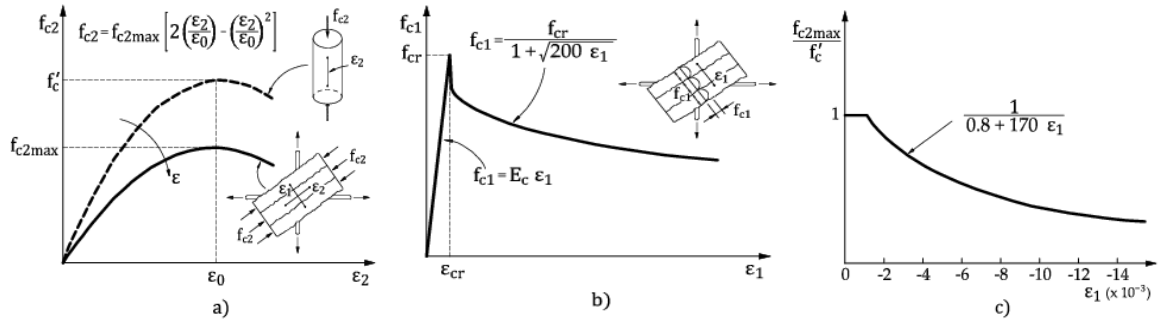

Fig. 3(a) Stress-strain relationship for cracked concrete in compression (ε_0=0.002), (b) maximum compressive stress as function of the principal tensile strain, (c) average stress-strain relationship for cracked concrete in tension (E_c=2·f_{c2max}/ε_0)

By means of the F.E.M., R.C. and P.C. beams are modelled as membranes structures, having non-linear behaviour and being susceptible of cracking. The general hypotheses and the biaxial stress-strain relationships according to the Modified Compression Field Theory (MCFT) are assumed (Vecchio and Collins 1986, Vecchio 1989, Bontempi *et al.* 1996, Sgambi 2004, Sgambi *et al.* 2006, Zhang *et al.* 2012, Palermo *et al.* 2014, Sgambi *et al.* 2014).

The MCFT considers a constant thickness membrane element, made of a matrix of concrete and reinforced by two orthogonal orders of bars. No overall slip between reinforcement and concrete is considered. The element has finite size, but it is treated as an infinitesimal: within the element, the stress field is constant and, during deformations, the boundary edges move and rotate remaining straight. For a given membrane state of stress or strain, the relationships between the stresses acting on the edges and the corresponding strains comply with following hypothesis:

1. The R.C. is a non-linear composite elastic material.
2. Equilibrium and compatibility are formulated in terms of average stresses and average strains, referred to areas which are sufficiently wide to contain a defined crack pattern.
3. In a general biaxial state, the direction of the principal compression strain ε_1 and that of the principal compression stress f_{c1} are correlated in a narrow band ($\theta_c \cong \pm 10°$). Therefore, we assume that the principal strain axes and the principal stress axes coincide.
4. Prior to the cracking strain ε_{cr}, the principal tensile stress f_{c1} is linear with ε1 and with an initial tangent modulus E_c. After ε_{cr}, in order to take the tension stiffening effects into account, f_{c1} decreases with the increasing values of ε_1, as shown in Figs. 3(a) and 3(b).
5. The principal compressive stress f_{c2}, corresponding to the principal strain ε_2, depends on the strain softening effect, due to the principal tensile strain ε_1. The strength $f_{c2,max}$ diminishes with ε_1 and the stress-strain relationship changes in affinity with $f_{c2,max}$, as shown in Fig. 3(c).
6. For the reinforcement, bilinear elastoplastic stress-strain relationships are assumed.
7. The possibility of transmitting the average tensile stress f_{c1} across the cracks has to be verified.

3.2 Tension stiffening in the membrane states

In a cracked R.C. element (Fig. 4(a)), the tensile stress at a crack is zero in the concrete, and it is maximum in the reinforcement (f_{sx}=$f_{sx,cr}$; f_{sy}=$f_{sy,cr}$). Between the cracks, the tensile stresses are

Expanding in Taylor's series the equations that compute the carbonation depth and the chloride concentration over time, with respect to the time *t*, we obtain following result from Eq. (3)

$$x(t+\Delta t)=x(t)+\frac{dx(t)}{dt}\cdot\Delta t+o\left(t^2\right)=x(t)+\left(\frac{25\cdot w'(t)\cdot\sqrt[4]{t}}{\sqrt{w(t)}}+\frac{25}{2}\cdot\frac{\sqrt{w(t)}}{\sqrt[4]{t^3}}\right)\cdot\Delta t+o\left(t^2\right) \tag{16}$$

and, from Eq. (7)

$$\begin{aligned}&C(x,t+\Delta t)=C(x,t)+\frac{dC(x,t)}{dt}\cdot\Delta t+o\left(t^2\right)=\\&=C(x,t)+C_0\cdot\frac{2}{\sqrt{\pi}}\cdot\frac{\left[D_{cr}\cdot w'(t)\cdot t+D_{cr}\cdot w(t)+D_{app}\cdot S_{m\theta}\right]\cdot x}{4\cdot t\cdot\left[D_{cr}\cdot w(t)+D_{app}\cdot S_{m\theta}\right]\cdot\sqrt{\left(D_{app}+\frac{w(t)}{S_{m\theta}}\cdot D_{cr}\right)\cdot t}}\cdot E_{ws}\end{aligned} \tag{17a}$$

where

$$E_{ws}=\exp\left[-\left(\frac{x}{2\cdot\sqrt{\left(D_{app}+\frac{w(t)}{S_{m\theta}}\cdot D_{cr}\right)\cdot t}}\right)^2\right]\cdot\Delta t+o\left(t^2\right) \tag{17b}$$

The rate of cracking *w'* is difficult to determine. Moreover, sensitivity analyses showed that its influence on the updated values of $x(t+\Delta t)$ and on $C(x, t+\Delta t)$ is little. Hence, it has been neglected in these computational model.

4.2 Criteria for sampling the structural behavior over time

From the mechanical point of view, the measure of damage is given by the reduction of the bearing area of reinforcing and prestressing steel. During the analysis, these areas are updated over time according to the evolution of the influence of the aggressive agents causing corrosion.

The sequence of the analysis is organized as follows:

• Environmental and material data, necessary to define the constant *K* in Eq. (2) and the constants C_s, D_{app} and D_{crk} in Eq. (7), are given.

• The structure is completely defined in geometry, mechanical materials characteristics and prestressing intensity.

• A sustained constant load is assumed. The load intensity is a percentage of the ultimate one, close to the permanent load in a bridge structure (for example 60%).

• The analysis starts and is repeated over time, according to assumed time intervals. For each step of analysis, displacements, cracking patterns, compressive and tensile stress are stored and filtered for significant control sections.

Further details will be given for the cases studied in the following.

5. Validation of the model

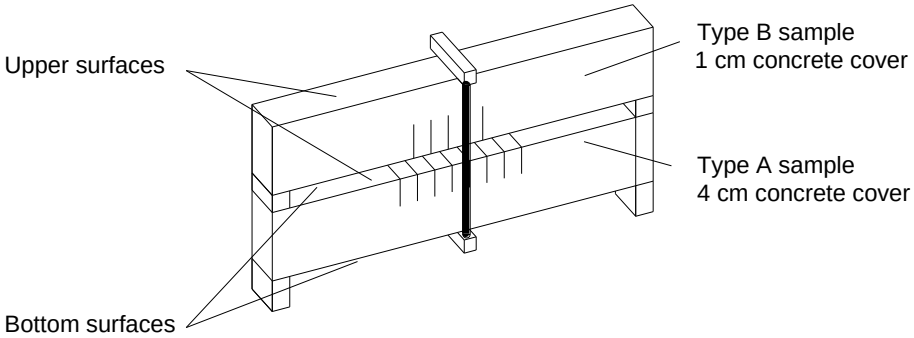

Fig. 6 LMDC beams (Castel *et al.* 1999). Loading system in three-points flexion

5.1 Modellization of the carbonation and chloride penetration

In the '80/'90 of the past century, a wide experimental program on the effects of the aggressive environmental agents on the mechanical behaviour of R.C. beams had been carried out (Castel *et al.* 1999, Castel *et al.* 2000, Vidal *et al.* 2007) at the Laboratoire Matériaux et Durabilité des Constructions (LMDC), Tolouse (France). Within the LMDC tests, we consider a set of rectangular beams having the same overall dimensions, but different cover thickness (Fig. 5), and subjected to constant concentrated loads, sustained for 13 years under different exposure conditions. Tables 1 and 2 summarize, respectively, the characteristics of the materials and the beam dimensions.

The beams were tested in couples (A1 with B1, A2 with B2), according to the setup shown in Fig. 6. One couple of specimens was exposed to natural weather conditions, but protected from rain, in order to study the development of carbonation. Another couple was maintained in a confined environment containing chloride, in order to study the influence of this specific chemical agent on the corrosion of the reinforcement.

In the following, the experimental results will be compared with the numerical ones, developed according to the model proposed in the previous paragraphs.

5.1.1 Penetration of carbonation in a progressive cracking pattern

We consider the couple of beams A2 and B2, exposed to natural weather conditions and subjected to the same load for the same time (13 years). Under these conditions, we expect that the different cover thicknesses (c_A=40 mm, c_B=10 mm), the different response to cracking and the different distribution of cracking along the span cause perceptible differences in the penetration of the carbonation. The depth of carbonation was experimentally measured every 20 cm along the intrados of beam B and along the extrados of beam A, in the fields between the couples of stirrups, in order to avoid local interferences from the steel bars.

The F.E. models of the beams are shown in Figs. 7(a), (b). Based on the characteristics of the cement paste and of the concrete mix, a coefficient of carbonation K=3.3 mm/year$^{1/2}$ and a corrosion rate i_{corr}=0.055 mm/year have been assumed in the analysis.

The results are shown in Figs. 7(a) and 7(b). Each figure shows: (i) the comparison between carbonation depths measured along the beam and obtained respectively from the experimental measurements and the F.E. analysis; (ii) the comparison between the corresponding crack patterns. In both beams the F.E. model is suitable to foresee how the depth of carbonation increases from

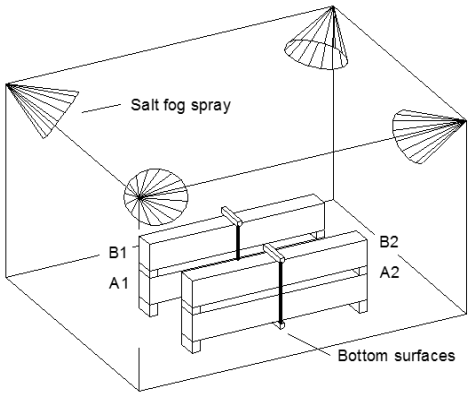

Fig. 8 LMDC beams (Castel *et al.* 2000). Experimental room and loading system in three-points flexion

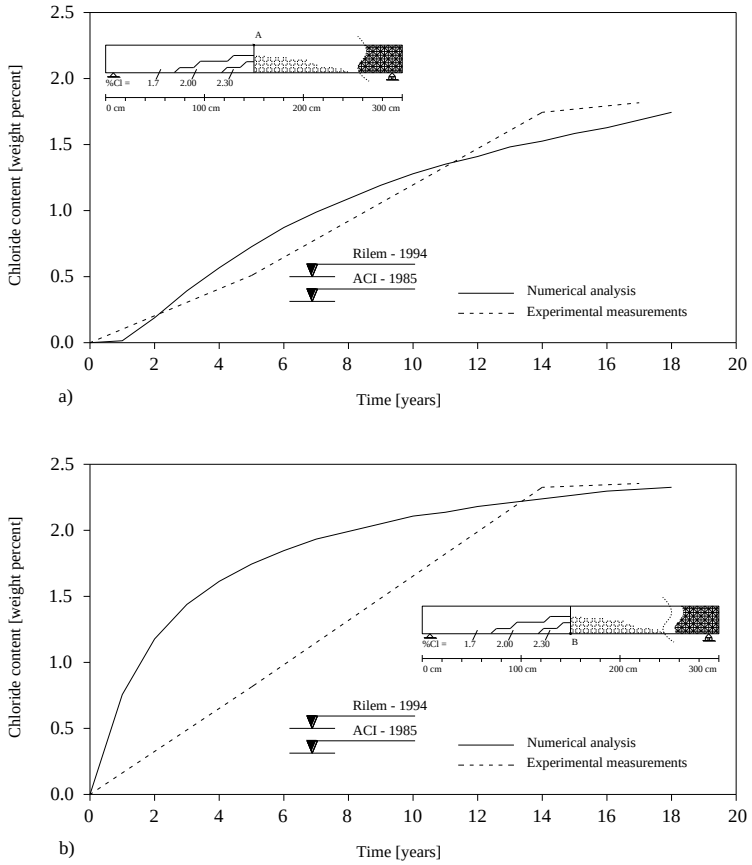

Fig. 9 Variation per years of chloride content at the depth of the reinforcement (16 mm) in the compression zone (a) and in the tension zone (b) of the corroded beam. Comparison between the numerical analysis and the experimental results obtained by Castel *et al.* (2000)

The chloride content was measured at midspan and at the depth of the compressed and tensioned fibres, i.e., at the level of the reinforcement bars.

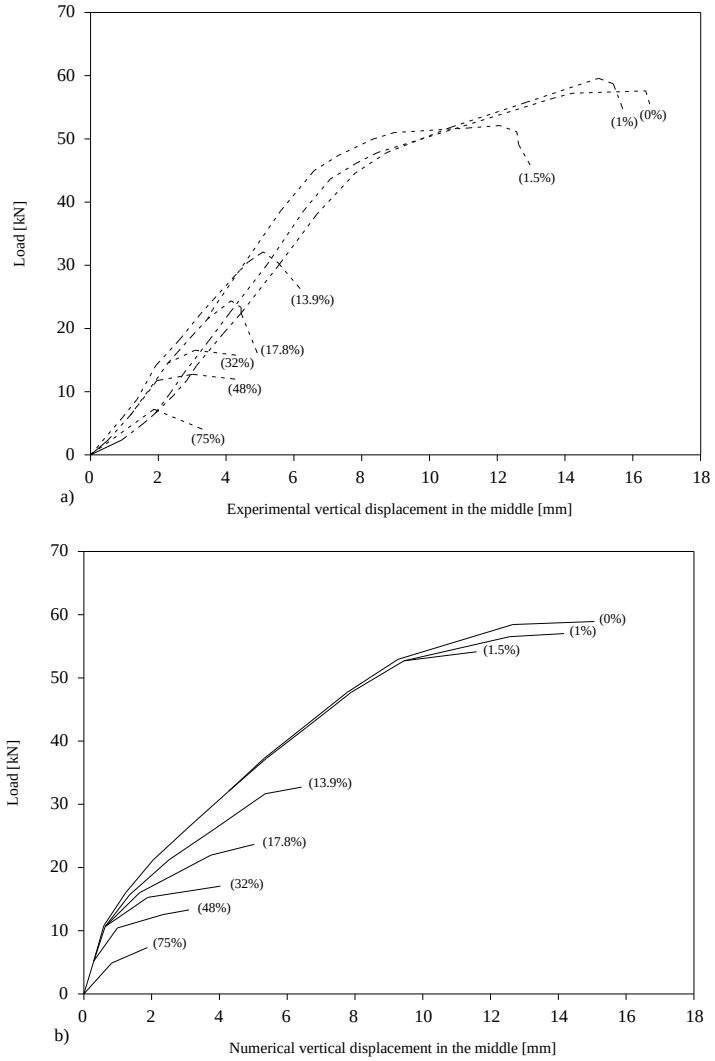

Fig. 10 Comparison between the numerical analysis and the experimental results obtained by Almusallam (1996). Load-displacement curves at different percentages of reinforcement corrosion: (a) Experimental tests; (b) numerical analysis

slightly cracked in the middle.

The numerical simulation of the chloride diffusion and of the corrosion process started from this initial condition. When the corrosion degrees reached one of the different levels considered in the experiments, the load was progressively increased until collapse.

Fig. 10(a) shows the experimental load-displacement curves at different percentages of reinforcement corrosion. Fig. 10(b) shows the corresponding curves obtained through the numerical analyses.

The model agrees with the experiments in representing how the progressive corrosion of the bars causes a corresponding reduction of the overall ductility and of the bearing capacity of the beams. In addition, the corresponding maximum load levels appear well approximated as well.

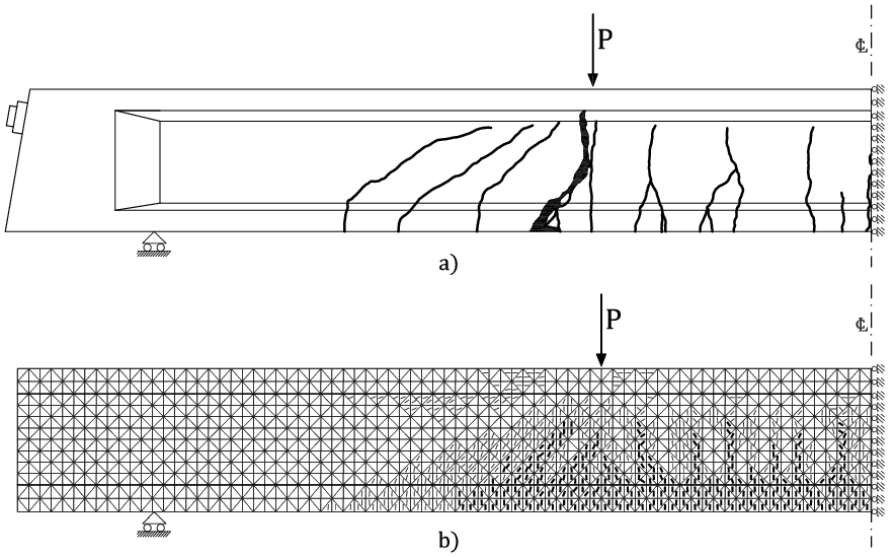

Fig. 12 Beam RI 5. Comparison between experimental (a) and numerical (b) crack patterns and between failure modes at the ultimate load P_u=82 kN (undamaged beam)

We refer to a prestressed concrete beam, called RI 5, belonging to a set of prestressed beams tested by Radogna (1965) at "La Sapienza", Università di Roma (Rome) in 1960s. The geometry of the beam, the reinforcement layout and the tendon profile are shown in Fig. 11. The characteristics of the materials shown in Table 5 have been used.

6.1 Undamaged beam

Initially, the beam was studied without damage alterations in order to check the reliability of the mechanical solver only. Under an increasing loading, a systematic comparison among the numerical and experimental results was carried out. Comparisons regarded displacements, the onset and the propagation of cracking, the load deflection curve and the ultimate load. Fig. 12 shows a comparison between the experimental and numerical crack patterns and collapse mechanism at the ultimate load (P_u=82 kN)

6.2 Corrosion scenarios

We refer to the typical microclimate conditions surrounding a bridge girder and to the data recorded during years of survey activity on existing bridges. The external surfaces of the structural elements are considered as uniformly exposed to the carbon dioxide present in the atmosphere and hence the carbonation process is considered always active.

As noticed during the surveying activities, the worse damages on a bridge beam frequently happen in proximity of certain particular sections, where joints, niches or ducts belonging to the drainage system allow infiltration and stagnation of water or liquids containing deicing salts. So, the chloride attack is assumed as localised in narrow bands, where the chloride concentration is assumed to be distributed according to a bell distribution, having vertical axis at the middle of the band and given by Eq. (18)

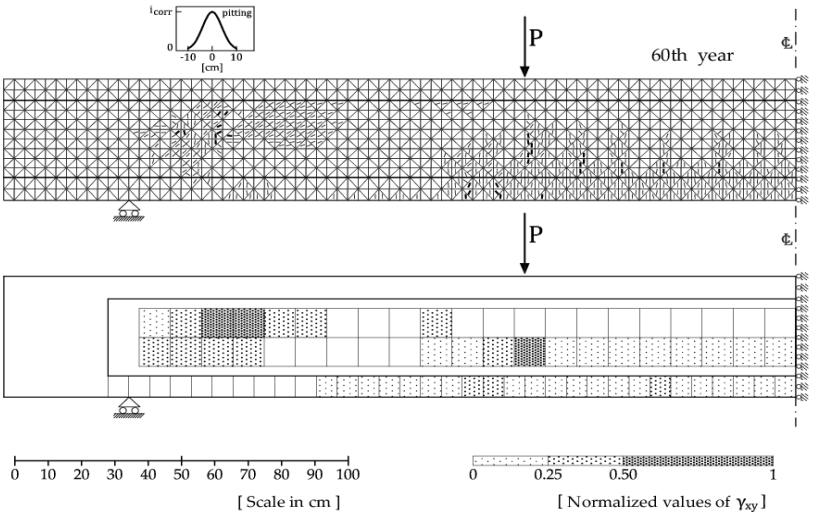

Fig. 13 Beam RI 5. Corrosion scenario CS1. Crack patterns and macrodivision of the shearing strain γ_{xy}, showing the failure mode at the onset of the collapse

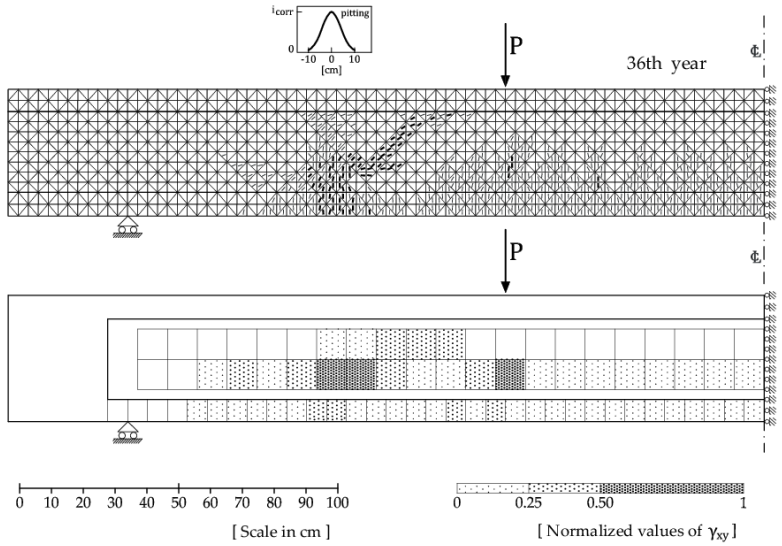

Fig. 14 Beam RI 5. Corrosion scenario CS2. Crack patterns and macrodivision of the shearing strain γ_{xy}, showing the failure mode at the onset of collapse

Fig. 16(a) shows how, as in the previous case, the corrosion starts after 24 years, while the tendom section decreases until the 36th year, when it reaches its breaking point (Fig. 16(a)). The displacement at midspan starts to increase after five years (Fig. 16(b)). However, in this case, when tendon breaks, the displacement diverges and the beam fails suddenly. The failure mode is not yet flexural, as in the undamaged beam. In the shear span, large shearing strains occur and the crack pattern shows newly-formed cracks, with a 45° orientation in the shear zone. Hence, a localized attack causing the corrosion of the tendon at the shear span changes the failure mode of the beam, which switches from flexural to shear type.

6.2.3 Corrosion scenario CS3 (uniform carbonation and chloride attack at the midspan)

The carbonation is assumed to be uniform, while the band attacked by chloride is about 200 mm wide and localized across midspan. Fig. 15 shows the crack patterns and a macrodivision of the shearing strain γ_{xy} at the onset of the collapse.

As shown in Fig. 16(a), corrosion starts after nine years and the tendon section vanishes in at the 18^{th} year. The displacement at midspan starts to increase after five years. After the 9^{th} years, the displacement rapidly increases until the beam collapse, which occurs after 18 years. As one can see from Fig. 15, the failure mode remains flexural.

6.3 A comparison among the mechanical behavior in the three scenarios

As already shown, Fig. 16(a) summarizes the reduction over time of the sectional area of the prestressing tendon and Fig. 16(b) summarizes the increment over time of the mid-span displacement for the different scenarios CS1 CS3.

The onset of corrosion and the collapse caused by corrosion happen quite early when the attack occurs at midspan. Such a behavior can be attributed to the presence of more severe flexural cracks in the middle of the beam when a localized attack takes place. This accelerates the reinforcement degradation process with respect to the other scenarios, in which the attack occurs in areas not yet exhibiting cracks.

It is also important to compare the different collapse modes. Beam RI 5 was designed so that the collapse mechanism would be flexural. The macro division of the shearing strain zones, shown in Figs. 13-15, contributes in highlighting how the corrosion of the tendon may contribute in switching the failure mode from flexural to shear.

7. Conclusions

This paper presents a computational approach to the analysis of reinforced and prestressed concrete elements under long-term loading conditions, and subjected to given damaging scenarios. The effects of the diffusion of aggressive agents, of the onset and the development of the corrosion state in the reinforcement and the corresponding mechanical response are studied. As known, the corrosion on the reinforcing bars influences the damaging rate in the cracking pattern evolution; hence, the damage development and the mechanical behaviors are considered as coupled phenomena.

The model reliability is validated in studying the diffusion of the aggressive agents and the corresponding changes in the mechanical response of simple structural elements against experimental data is reported in Literature. These elements consist of simply supported reinforced concrete beams, subjected to carbonation and chloride. The benchmarks show how the analysis is able to reproduce the penetration rate of carbonation and chlorides at different levels of cracking, the progression of the steel corrosion process, the evolution of the cracking pattern and the influence of all those factors on the ultimate load carrying capacity.

A second set of applications concerns the behavior of a P.C. beam exposed to the attack of chlorides and carbonation. At first, the beam is studied in its sound state, for which the result of the experimental test are available. Then, the same beam is analyzed in damaged states, described by three different attack scenarios. The analyses highlight the influence of the degradation process on the non-linear response of the structure and on its failure mode. In particular, it is shown how,

Isecke, B. (1983), "Collapse of the Berlin congress hall prestressed concrete roof", *Mater. Perform.*, **21**(12), 36-39.
Jacobsen, S., Sellevold, E. and Matala, S. (1996), "Frost durability of high strength concrete: Effect of internal cracking on ice formation", *Cement Concrete Res.*, **26**(6), 919-931.
Köliö, A., Pakkala, T.A., Lahdensivu, J. and Kiviste M. (2014), "Durability demands related to carbonation induced corrosion for Finnish concrete buildings in changing climate", *Eng. Struct.*, **62-63**, 42-52.
Lu, Z.H., Ou, Y.B., Zhao, Y.G. and Li, C.Q. (2016), "Investigation of corrosion of steel stirrups in reinforced concrete structures", *Constr. Build. Mater.*, **127**, 293-305.
Malerba, P.G. (2014), "Inspecting and repairing old bridges: Experiences and lessons", *Struct. Infrastruct. Eng.*, **14**(4), 443-470.
Malerba, P.G. and Sgambi, L. (2014), "Riveted steel elements deformed by the swelling of interstitial rust. A study on a residual bearing capacity", *Proceedings of the 7th International Conference on Bridge Maintenance, Safety and Management*, Shanghai, China, July.
Malumbela, G., Alexander, M. and Moyo, P. (2009), "Steel corrosion on RC structures under sustained service loads-a critical review", *Eng. Struct.*, **31**(11), 2518-2525.
Michel, A., Otieno, M., Stang, H. and Geiker, M.R. (2016), "Propagation of steel corrosion in concrete: Experimental and numerical investigations", *Cement Concrete Compos.*, **70**, 171-182.
Nürnberger, U. (2002), "Corrosion induced failure mechanisms of prestressing steel", *Mater. Corros.*, **53**(8), 591-601.
Otsuki, N., Miyazato, S., Diola, N.B. and Suzuki, H. (2000), "Influences of bending crack and water-cement ratio on chloride-induced corrosion of main reinforcing bars and stirrups", **97**(4), 454-464.
Palermo, A., Gil-Martin, L.M., Hernandez-Montes, E. and Aschheim, M. (2014), "Refined compression field theory for plastered straw bale walls", *Constr. Build. Mater.*, **58**, 101-110.
Paulík, P., Bacuvcík, M., Ševcík, P. and Janotka, I. (2016), "Material properties and carbonation depths measured on seven, more than a 100-years old concrete bridges in Slovakia", *Proc. Eng.*, **156**, 326-333.
Radogna, E.F. (1965), *Nota Informativa su Esperienze in Corso sul Comportamento a Taglio di Travi Precompresse a Cavi Post-Tesi, Atti delle Giornate del Precompresso*, Ravello, 24-30.
Sarja, A. and Vesikari, E. (1996), *Durability Design of Concrete Structures*, RILEM Report Series 14, RILEM Technical Committee 130-CSL, E & FN Spon, London, U.K.
Schiessl, P. and Lay, S. (2005), *Influence of Concrete Composition, Corrosion in Reinforced Concrete Structures*, Woodhead Publishing, Cambridge, 91-134.
Sgambi, L. (2004), "Fuzzy theory based approach for three-dimensional nonlinear analysis of reinforced concrete two-blade bridge piers", *Comput. Struct.*, **82**(13-14), 1067-1076.
Sgambi, L. (2014), "Influence of degradation at the base of a support post in a collapse of an old guardrail: A forensic analysis", *Eng. Fail. Anal.*, **42**, 284-296.
Sgambi, L., Bontempi, F. and Garavaglia, E. (2006), "Structural response evaluation of two-blade bridge piers subjected to a localized deterioration", *Proceedings of the 3rd International Conference on Bridge Maintenance, Safety and Management*, Porto, Portugal, July.
Sgambi, L., Gkoumas, K. and Bontempi, F. (2014), "Genetic algorithm optimization of precast hollow core slabs", *Comput. Concrete*, **13**(3), 389-409.
Tuutti, K. (1982), *Corrosion of Steel in Concrete*, CBI Research Report No. 4.82, Swedish Foundation for Concrete Research, Stockholm, Sweden.
Val, D.V., Stewart, M.G. and Melchers, R.E. (1998), "Effect of reinforce corrosion on reliability of highway bridges", *Eng. Struct.*, **20**(11), 1010-1019.
Vecchio, F.J. (1989), "Non-linear finite element analysis of reinforced concrete membranes", *ACI Struct. J.*, **86**(1), 26-35.
Vecchio, F.J. and Collins, M.P.C. (1986), "The modified compression-field theory for reinforced concrete elements subjected to shear", *ACI Struct. J.*, **83**(2), 219-231.
Vesikari, E. (1988), "Service life prediction of concrete structures with regard to corrosion of reinforcement", Research Report NA 553, Technical Research Center of Finland (VTT), Finland.
Vidal, T., Castel, A. and François, R. (2007), "Corrosion process and structural performance of a 17 year old

reinforced concrete beam stored in chloride environment", *Cement Concrete Res*., **37**(11), 1551-1561.
Vořechovská, D., Podroužek, J., Chromá, M., Rovnaníková, P. and Teplý, B. (2009), "Modeling of chloride concentration effect on reinforcement corrosion", *Comput.-Aid. Civil Infrastr. Eng*., **24**(6), 446-458.
Woodward, R.J. and Williams, F.W. (1988), "Collapse of ynys-y-gwas bridge, west glamorgan", *Proceedings of the Institution of Civil Engineers*, Part I 84, 634-669.
Zhang, Y.F., Torgal, F. and Zhang, Y. (2012), "Shear behaviour of steel fibre reinforced self-consolidating concrete beams based on the modified compression field theory", *Compos. Struct*., **94**(8), 2440-2449.

CC

Appendix: Sectional area reduction due to pitting

Referring to Fig. 2, the following geometrical relationships between pit depth and reduced cross-sectional area of a rebar come out.

$$a(t) = 2 \cdot p(t) \cdot \sqrt{1 - \left[\frac{p(t)}{D_0}\right]^2} \tag{a}$$

$$\theta_1(t) = 2 \cdot \arcsin\left[\frac{a(t)}{D_0}\right] \tag{b}$$

$$\theta_2(t) = 2 \cdot \arcsin\left[\frac{a(t)}{2 \cdot p(t)}\right] \tag{c}$$

$$A_1(t) = 0.5 \cdot \left[\theta_1(t) \cdot \left(\frac{D_0}{2}\right)^2 - a(t) \cdot \left|\frac{D_0}{2} - \frac{p(t)^2}{D_0}\right|\right] \tag{d}$$

$$A_2(t) = 0.5 \cdot \left[\theta_2(t) \cdot p(t)^2 - a(t) \cdot \frac{p(t)^2}{D_0}\right] \tag{e}$$

$$A_{pit}(t) = \begin{cases} A_1 + A_2 & \text{se} \quad p(t) \le \dfrac{D_0}{2} \\ \dfrac{\pi \cdot D_0^2}{4} - A_1 + A_2 & \text{se} \quad \dfrac{D_0}{2} < p(t) \le D_0 \\ \dfrac{\pi \cdot D_0^2}{4} & \text{se} \quad p(t) > D_0 \end{cases} \tag{f}$$

$$A_s(t) = \frac{\pi \cdot D_0^2}{4} - A_{pit}(t) \tag{g}$$